Proceedings World Geothermal Congress 2020+1
Reykjavik, Iceland, April - October 2021

Imaging Faults Within Geothermal Systems From 3-D MT Inversion: A Comparison Between Smooth And Blocky 3-D Approaches

Flora F. Solon(1), Sophie Hautot(2), Pascal Tarits(1,2), Sebastien Haffen(3)

1 IUEM, UMR 6538 Laboratoire Geoscience Ocean, Plouzané, F29280, France

2 IMAGIR Sarl, Saint Renan, France

3 TERANOV Sas, Guadeloupe, France

flora.ferreirasolon@univ-brest.fr

Keywords: Magnetotelluric, 3D inversion, Geothermal, Fault system

ABSTRACT

Because geothermal systems produce strong variations in underground electrical conductivity, electromagnetic methods such as magnetotellurics (MT) have become commonly used in geothermal reservoir exploration. Over the last years, several imaging methods for MT data have emerged. These methods can use different mathematical approaches (finite differences, finite elements or integral equations) to provide an estimate of the 3D resistivity distribution within the subsurface. Here we use field data sets to study the capacity of two end members 3D MT imaging methods to characterize some key features of geothermal systems. The two methods we applied have been developed to obtain solutions using different ways of parameterizing the subsurface, regularization and inversion strategies. The main difference relies in the relationship between constraints and unknowns, or simply, data and parameters. They have been characterized as over-determined inverse problem (ODIP) in which the number of data is larger than the number of parameters, and under-determined inverse problem (UDIP) when the number of parameters is larger than the number of data. We demonstrate that the resulting images obtained by both methods can describe the main structures of the geothermal system such as the clay cap, heat source and faults system. Differences lay in the resolution power of the different techniques. UDIP models tend to generate shallow features (bubble like) and to produce smooth distributions at depth. The UDIP inversion method gives good results for areas where the subsurface resistivity changes in a gradual manner. This is related to the large number of parameters used and the mesh size, which needs to be small. In contrast ODIP models present stronger and continuous conductors and resistors. The model features tend to be blocky but the ODIP inversion method gives significantly better results where there are sharp boundaries. It is able to recover the main strikes of the geothermal fault system. The horizontal resolution of both methods can be limited due to site spacing however the obtained results from each of the approaches present stable solutions, fit to the data and general agreement.

1. INTRODUCTION

In recent years, there has been an increasing interest in the development and use of three-dimensional (3D) electrical imaging surveys. Such surveys have been successfully used in several complex environments such as geothermal systems (Bibby et al., 2009; Muñoz, 2014; Gao et al., 2018; Samrock et al., 2018) where other geophysical methods are traditionally used. Geological units related to geothermal sources induce large variations in the electrical conductivity of the subsurface, due to water content, porosity, salinity of pore fluids and alteration of mineralogy (e.g. Spichak and Manzella, 2009). The presence of faults, for example, plays an important role in geothermal systems. They can behave as pathways to geothermal fluids increasing the permeability controlling flow rate, direction and fluid infiltration. Geothermal fluids have high concentrations of dissolved salts, increasing the conductivity within a rock matrix. The temperature also contributes to changes in conductivity of the fluids and the rock matrix. High temperatures for example, leads to a significantlarge reduction in the bulk resistivity. Hydrothermal alterations usually lead to the formation of highly conductive conductive clays caps (illite, smectite, montmorilonite) over a wide temperature range from under 100°C to 200°C. At temperatures over 220 − 240°C, alteration is mainly in form of chlorite and epidote minerals, showing higher resistivity values than the clay cap. Thus, an increase in resistivity beneath a highly conductive clay cap, reflecting an increase in temperature with depth, is a common signature of high-temperature geothermal systems.

In order to image the subsurface and characterize the geological units inside a geothermal system, different inversion routines may be used to determine the resistivity and provide model responses that agrees with the observed data. A number of inversion techniques have been applied in the interpretation of MT data (e.g. Mackie and Madden, 1993; Newman and Alumbaugh, 2000; Siripunvaraporn et al., 2002; Hautot et al., 2000; Avdeev, 2005; Egbert and Kelbert, 2012). These methods choose different mathematical approximations to the problem (finite differences, finite elements or integral equations), different strategies to construct and constrain the solution and different approaches to parameterize the subsurface.

This study examines two inversion methods set out to obtain solutions using different ways of parameterizing the subsurface, regularization and inversion strategies. One of the main difference relies in the relation between constraints and unknowns, or simply, data and parameters. We refer to these methods as over-determined inverse problem (ODIP) and under-determined inverse problem (UDIP). Both are iterative, providing a solution in several steps. We analyze and compare the methods under three points of view: *i*) strategy used to solve the MT inversion problem; *ii*) number of unknowns vs number of data; *iii*) their ability to extract important properties and features of geothermal systems, such as faults, clay cap, intrusions, deep sources.

To compare both methods we used a field data set from a MT survey carried in the Sol de Mañana geothermal system, Bolivia (JICA, 2015) (Figure 1). We show that 3D MT inversion can provide a geological meaningful image of the main structures present

in the geothermal system. Additionally, the MT data can also provide important information about the fault system which control the flow and distribution of geothermal fluids.

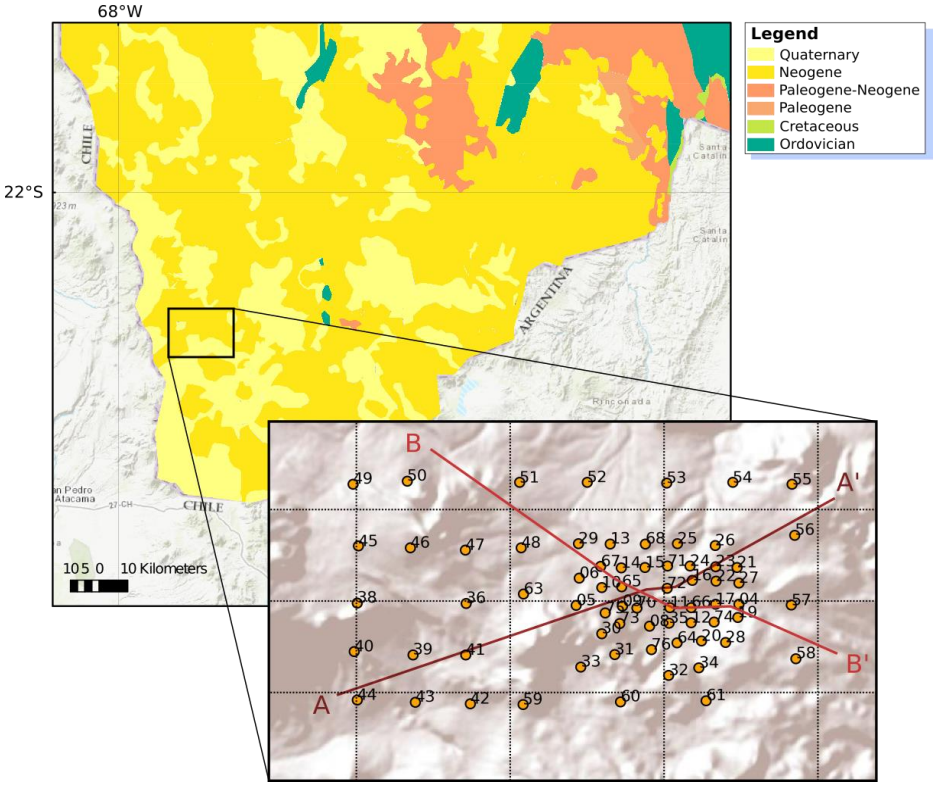

Figure 1: Geological map of Southern Bolivia (SERGEOMIN 2019), with emphasis on the area of Sol de Mañana geothermal system (JICA, 2015, JOGMEC, 2011). The orange circles illustrate the position of the MT sites and the lines represents the MT profiles AA' and BB'.

2. TRI-DIMENSIONAL MAGNETOTELLURIC INVERSION

The inversion process aims at estimating a resistivity distribution within the subsurface based on real observations of the MT data. The responses are given at specific locations and frequencies. Thus, solving the inverse MT problem involves finding one or more resistivity models that reproduces the observed data within their error. In most cases, the inversion process seeks to minimize the residuum between observed and predicted data, known as the penalty function (or misfit function).

Distinct approaches can be applied to minimize the penalty function. Over the last decades, several three-dimensional (3D) inversion codes have been developed and were applied to real data (e.g. Avdeev, 2005; Heise et al., 2008; Newman et al., 2008; Avdeev and Avdeeva, 2009; Bibby et al., 2009; Munoz et al., 2010; Siripunvaraporn, 2012; Kelbert et al., 2014; Coppo et al., 2018). The differences between them rely either in the parametrization of the Earth, regularization techniques or the chosen inversion strategy (Miensopust et al., 2013).

In this study, two different inversions methods were adopted. The inversion package ModEM (Modular Electromagnetic Inversion), developed by Egbert and Kelbert (2012) and Kelbert et al. (2014) and the inversion algorithm, Minim3D, developed by Hautot et al. (2000), Hautot et al. (2007). For clarity, they will be differentiated according to the relationship data/parameters. ModEM belongs to the techniques classified as an under-determined inverse problem (UDIP) since it uses a much larger number of parameters than the number of data. Minim3D, classified as over-determined inverse problem (ODIP) uses a number of parameters smaller than the number of data. Typical numbers for the ratio parameter/data are observed as > 10 for UDIP inversions and < 0.2-0.4 for ODIP inversion.

The inversion package ModEM uses the non-linear conjugate gradients (NLCG) method to solve the MT inverse problem in the model-space. NLCG is related to the linear CG method, which solves normal equations derived from a quadratic approximation of the penalty function. The NLCG method, however, directly minimizes the penalty function avoiding the iterative linearized inversion procedure (Rodi and Mackie, 2001). Gradient based inversion schemes such as NLCG, require accurate solutions to ensure precise computation of the called sensitivity matrix. Because the accuracy of the computed solution in the forward modeling depends mainly on the discretization of the subsurface, the dimension of the cells in the 3D grid must be kept small compared to the skin depth (Weaver, 1994) to ensure a good approximation of Maxwell's equations and to reduce numerical instability (Meqbel, 2009). However, keeping cell dimensions small causes a huge number of model parameters to be solved both in the forward modeling and the inverse problems. NLCG is a regularized inversion scheme and a smoothness criterion is commonly applied which often results in uniformly blurred features that tend to not appear geologically meaningfully. Several strategies may be used to choose a value for the regularization parameter to ensure that neither the data misfit term nor the smoothing term dominates the penalty function (e.g. Meqbel [2009]; Yang et al. [2015]).

The full 3-D MT inversion algorithm Minim3D (Hautot et al., 2000; Hautot et al., 2007) is based on the minimization of the misfit between the data and the model response using a non-linear steepest gradient method. The inversion is based on a local minimum search algorithm derived from Rosenbrock method (Rosenbrock, 1960). The approach allows to easily implement an inversion grid (IG) independent from the forward calculation grid (FCG), finer with adequate boundary conditions for accurate results. In practice, the IG is built by merging several cells of the FCG into larger blocks. The merging takes into account the data distribution and the resolution loss with depth. The inversion usually starts with a homogeneous half space and once a good agreement is obtained between the 3D model response and the data, a regularization factor is added to the error function and a new solution is searched again. The regularizing term controls the resistivity contrast between blocks and is the sum over all vertical and horizontal squared differences in the logarithm of the resistivity between two adjacent blocks (Hautot and Tarits, 2009). The benefit of this approach is that a minimum of the penalty function is found in a smaller number of calls to the forward solution than in NLCG approaches. In addition, unlike ModEM, the gradient of the penalty function is not required and it is not necessary to calculate the sensitivity matrix. Only the forward problem is solved at each iteration through the 3-D finite difference algorithm derived from Mackie et al. (1993).

3. FIELD DATA EXAMPLE

3.1 Geophysical, geological and geothermal context

Sol de Mañana of Laguna Colorada geothermal system is located in Southwest of Bolivia (Figure1). The tectonic structure of the Sol de Mañana can be characterized by two orthogonal fault systems in NW-SE and NE-SW directions (Terceros, 2000). The NW-SE faults are considered to be extended to depth and they are potentially serving as pathway for geothermal fluids to shallower areas and feeding the high-permeability and high-temperature reservoir of the field.

3.2 Magnetotelluric data

Seventy broad band MT soundings were carried out in the geothermal field area of Sol de Mañana, Bolivia (Figure 1). The MT data of this survey have been acquired by Teranov using Metronix data acquisition system. Five components of the time-varying, natural EM field have been recorded in three frequency bands, 4096, 2048 and 128 Hz: three components of the magnetic field (magnetic north Hx (t), magnetic east Hy (t) and magnetic vertical Hz (t)) and two horizontal components of the electric field (Ex (t) and Ey (t)). The electric and horizontal magnetic field time-series were processed using the robust remote reference method of Chave and Thomson (2003) (BIRRP - Bounded Influence Remote Reference Processing), to obtain, in the frequency domain, the 2 × 2 complex impedance tensor Z composed by the elements, Zxx , Zxy , Zyx and Zyy . The impedance tensor is usually converted into apparent resistivity and phase for the various observational frequencies or periods, providing information about the resistivity (or conductivity) for a non-uniform half-space Earth. An example of MT sites is shown in Figure 2.

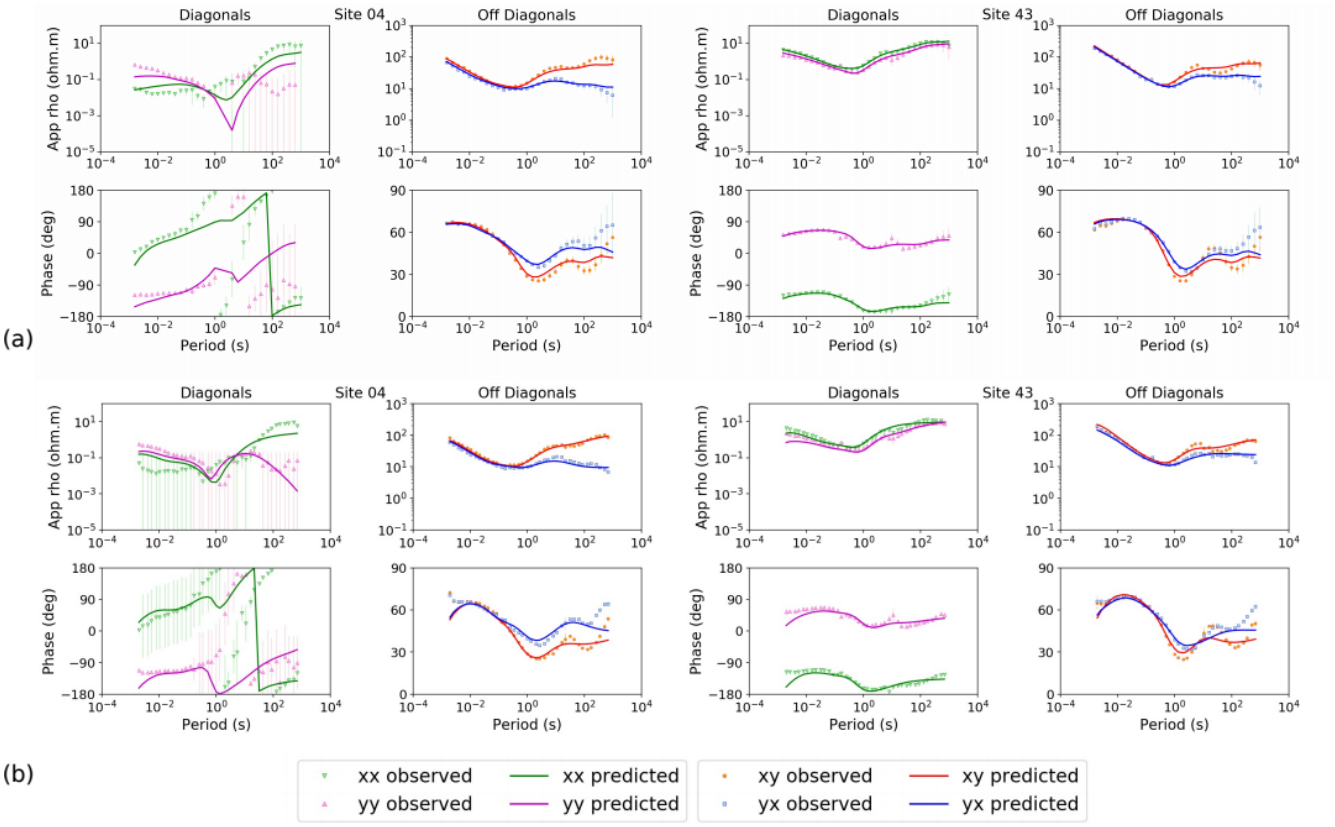

Figure 2: The MT impedance tensor from selected sites. Both the amplitude and phase of the diagonal and off-diagonal terms are shown. Amplitudes are expressed in apparent resistivity (Ωm), and phases (degrees). The solid line is the impedance predicted by the best-fitting 3-D model obtained from (a) UDIP method and (b) ODIP method. See Figure 1 for the site locations.

4. INVERSION RESULTS

The differences in the inversion parameters used in the 3D inversion of the data set using either ModEM code (UDIP) and Minim3D code (ODIP) are summarized in Table 1. In this section we show the final resistivity models and report the main features of the methods in terms of number of data and parameters, grid dimensions, type of regularization, error assignment, misfits and number of calls of the forward solution.

To compare the fit between the observed data and the model responses obtained from each inversion method, the root mean square (*rms*) values are computed in each step and/or iteration of each inversion method. The *rms* calculation considers the data errors weighted by an error-floor, adequately selected according to each inversion method. The minimization procedure stops when a target *rms* is obtained given a minimum error-floor (UDIP) or when the rms no longer change significantly (ODIP). The data weighting being different for each approach, the final rms considered satisfactory is different for UDIP and ODIP.

Table 1: Model parameters used in the 3D inversion of the data set using ModEM and Minim3D. The number of degree of freedom (NDF) here is understood to be the number of sites times the number of periods times 4 components of the impedance tensor times 2 for real and imaginary parts.

	ModEM - UDIP	Minim3D - ODIP
Approache	Egbert and Kelbert [2012]	Hautot et al. [2007]
NDF	15, 244	19, 652
Number of parameters	128, 968	4, 000
Layer thickness	Log increase after 1500 m	Log increase from surface
Number of frequencies	31	all available (31 to 38)
Frequencies per decade	5	N/A
Initial model	$60\Omega.m$	$60\Omega.m$
Inverted data	Full tensor	Full tensor
Topography	Yes	Yes
rms	3.2	5.5

4.1 Results using the UDIP method

Data set used in this inversion was formed by the non-rotated full impedance tensor components of 31 periods distributed on a logarithmic scale that varied from approximately 10^{-3} s to 10^{3} s. The total number of data is 15,244. A starting error floor of 10% were assigned in the first step of the inversion. After, this value decreased gradually to 1.5% for the off-diagonal elements and 3% for the diagonals.

The study started by using a fine model formed by a mesh of 53 × 83 × 53 cells totaling in 233,147 parameters to be estimated. The large number of parameters due to the small size of cells, associated with the UDIP method, leads to a concentration of resistivity features forming circular shapes around MT sites in the near-surface area. In an attempt to reduce this effect, a new inversion was realized with a coarser model formed by 49 × 56 × 47 cells with minimum dimension of 450 × 450 × 50 m. The total number of parameter to be estimated decreased to 128,968. To track the misfit obtained from each inversion method, the *rms* was computed for each step of inversion. A final *rms* of 3.2 was obtained for the best-fitting model, and an acceptable agreement between observed and predicted data is observed (Figure 2). Closer inspection of the data indicates good fit at shorter periods and some difficulty to fit the data at longer ones.

The results presented in this work are shown as horizontal and vertical sections of the resistivity distribution for different elevations in Figures 3a and 4a. The main electrical features in these model sections include a strong conductor with isolated resistive structures at 4,700m elevation above sea level (asl); a regional and smooth conductor at 3,800m asl and a very smooth model section showing no relevant electrical structures below 1,000m asl (Fig 5a). We observe that the electrical structures produced by the inversion using UDIP method tend to concentrate at near-surface while the deeper areas remain smooth then disappear below 1,000m asl (Figure 5a). This is evidenced by the flatness of the predicted data curves of some MT stations over longer periods, shown in Figure 2.

4.2 Results using the ODIP method

For this inversion we used the full MT tensor at all available periods and at all available sites, thus a larger number of data than for UDIP inversion (Table 1). The data error ranges from a minimum error floor of 1.5 and 3% of the impedance amplitude for the off-diagonal and the diagonal components respectively to the standard deviation obtained from the data processing. For the grid dimensions, an inversion grid (IG) independent from the forward calculation grid (FCG) was used. While the FCG grid is formed by a finer mesh composed by 20 × 29 × 15 cells with minimum dimension of 250 × 350 × 20 m, the IG is formed by a coarser one that may be updated during the inversion. The grid is easily refined around sites that show large misfits. For our study case, the final IG is composed of 4,000 parameters to be inverted, around 32 times less than the number of parameters necessary for the coarse UDIP inversion. An homogeneous starting model was adopted, with resistivity of 60 Ωm. The small number of parameters in the deeper layers associated with the ODIP method, leads to resulting models characterized by blocky features at depth. Final rms of 5.5 was obtained for the best-fitting model. The agreement between observed and predicted data for selected sites is shown in Figure 2.

Figures 3b and 4b provides the results obtained from the the ODIP inversion. From the model sections we can see the same conductor of Figure 3a, at 4700m asl, but the resistive feature seems stronger and more continuous. A regional and smoother conductor at 3800m asl is also observed in Figure 3b, comparable toto the UDIP result. Different patterns of main electrical structures are evidenced in the presented results: continuous structures at near-surface, blocky features and less smoothness at

deeper areas and structures below 0m asl (Figure 5b). This type of pattern is related with the relative small number of parameters used in the ODIP method.

5. INTERPRETATION OF THE 3D RESISTIVITY MODELS

The final 3D resistivity models obtained by both inversion methods are presented as horizontal sections in Figure 3 for elevations 4,700 and 3,800 m asl. The fault system plotted as black lines in Figure 3 was obtained in JICA (2015). We can observe that most faults are in the NW-SE direction, and some are displaced by faults in the NE-SW direction. The fault system control the conductive geothermal fluids in the Bolivia geothermal system.

In the plan section at 4700m asl in Figure 3, significant discontinuity between low and high values of resistivity are observed In this figure, we reported the fault system from JICA (2015). We can observe that most faults are in the NW-SE direction, and some are displaced by faults in the NE-SW direction. The fault system control the conductive geothermal fluids in the Bolivia geothermal system. The resistivity model for both UDIP and ODIP shows a zone of low resistivity that extends from the Southwestern toward the center, in a Northeastern direction, following the NE-SW faults. We observe a good agreement between the actual main faults and the transition between resistor and conductor in the resistivity models at 4,700m asl (Figure 3). The continuity of the large structures in the ODIP model (Figure 3b) seems in better agreement with the major faults than the UDIP model (Figure 3a) because the later tends to focus smaller scale structures. The main fault strikes are also visible at 3800m asl. At this depth, both resistivity models are in better agreement.The low resistivity values are attributed to geothermal fluids controlled by the fault system as observed in Figure 3. This zone characterizes the top of the smectite clay cap alteration zone (JOGMEC, 2011; JICA, 2015; Villarroel-Camacho, 2014). The low resistivity anomaly is surrounded by a resistive zone. The general area of the geothermal reservoir is highlighted by white dashed lines in Figure 3, obtained in JICA (2015). We observe the hydrothermal alteration zone characterized by low resistivity values in the same area. The horizontal sections illustrating elevation 3,800 m, at Figure 3, evidences the lateral range of the clay cap layer, characterized by a low resistivity zone. We can observe its extension in depth in depth in Figure 4, reaching approximately 1 km thick. Between MT sites 041 and 075, it appears to be exposed at the surface, reaching a thickness of 1.5 km. Enhanced resistivity within the cap rock layer is observed in the central region of the model, in the reservoir area (Figure 3).

The vertical resistivity sections in Figure 4 highlight the main characteristics of the geothermal system. Information about the temperature and composition of the geothermal field was obtained through boreholes located in the central part of the study area (Villarroel-Camacho, 2014). Temperatures of 200°C are observed within the clay cap layer as showed in Figure 4. Enhanced resistivity within the cap rock layer is observed in the central region of the model, in the reservoir area (Figures 3-4). The vertical sections reveal its extension in depth beneath the conductive clay cap, stressed by the label S1. Both UDIP and ODIP models agree on the main features. The difference between the two approaches is clearly visible. The UDIP model shows a very smooth distribution of resistivity while the blocky structure of the ODIP model outlines well the strong resistivity contrasts, both laterally and vertically. In particular, it is possible to suggest how the surface fault may extend in depth (Figure 4b). The increased resistivity values correlates with the high temperature (240°C) heat source rocks. S1 is emplace between normal faults between MT sites 075 and 072 in profile AA' and 067 and 065 in profile BB'. What stands out in Figure 4 is the clear discontinuity in all resistivity models around this area. This discontinuity, however, seems more evident in the ODIP models (Figure 4b), particularly in profile AA'. From the vertical sections shown in Figure 5, we observe that the resistive feature, interpreted as the source rock, is clearer in the ODIP models, as for the UDIP models, it appears as a weak and smooth structure.

These results are in agreement with the premises of the used inversion methods. Due to the large number of parameters, the UDIP method tends to produce isolated shallow resistive features as observed in the resistivity model at elevation 4,700m asl (Figure 3a). These features are most likely continuous, as suggested by the ODIP model (Figure 3b), and characterizes the volcanic rocks present at shallower areas of Sol de Mañana field. Moreover, at depth, the UDIP method produce smoother distributions of resistivity. This makes it difficult to differentiate of discontinuities and the characterization of faults and strike directions. The number of parameters close to the number of data in the ODIP method generates blocky structures but it is able to better recover discontinuities in the resistivity distribution.

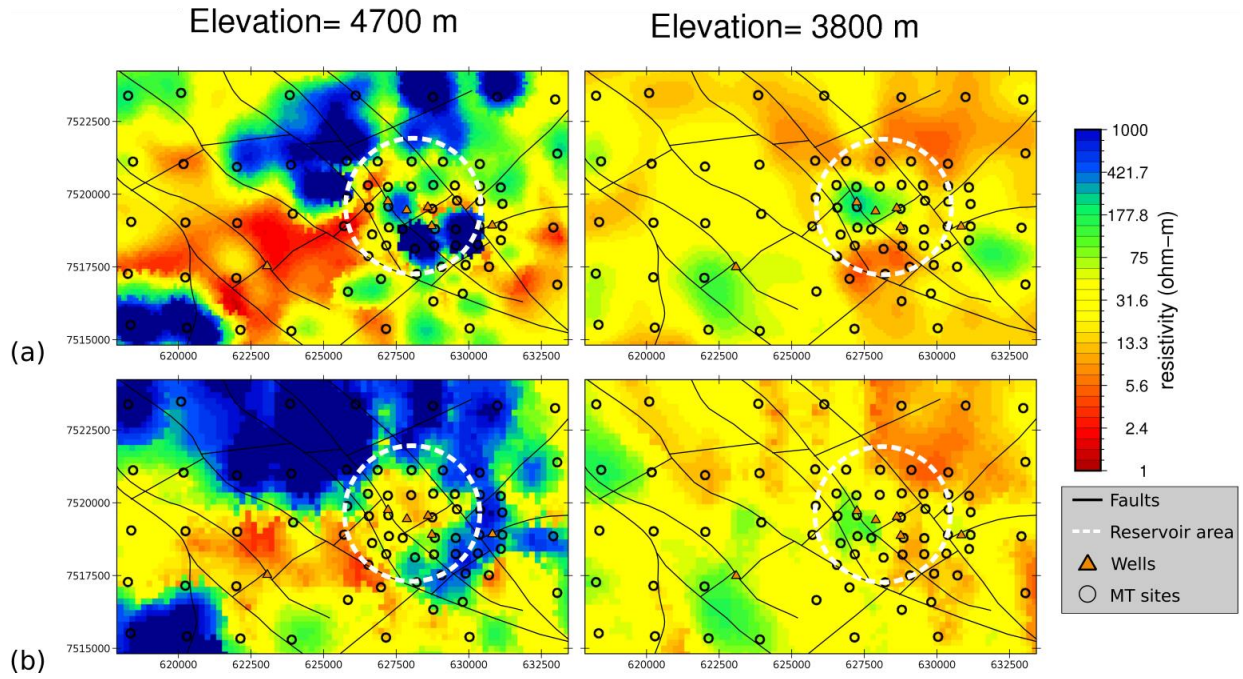

Figure 3: Plane view showing the resistivity distributions at elevations 4700, 3800 obtained using (a) UDIP method and (b) ODIP method. The circles represent the MT sites, black lines represent the surface fault system of the area and the white dashed lines represent the interpretation of the geothermal reservoir.

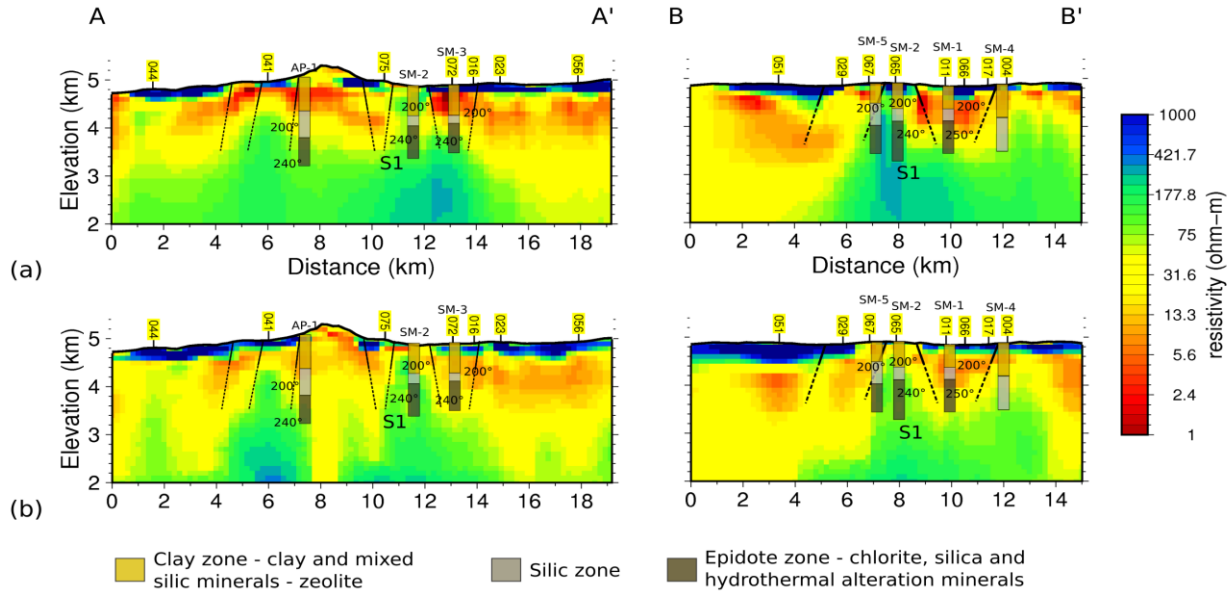

Figure 4: Plane vertical resistivity sections showing the resistivity distributions along profiles AA' and BB' (Figure1). (a) UDIP inversion method and (b) ODIP inversion method. The black lines represent the interpreted faults of the survey area extrapolated in depth as dashed lines. We reported the data from the boreholes (geological columns as well as the temperatures) in JICA (2015) and Villarroel-Camacho (2014). Observe that high temperatures correlates to the high resistivity area identified as the heat source S1 associated with the reservoir.

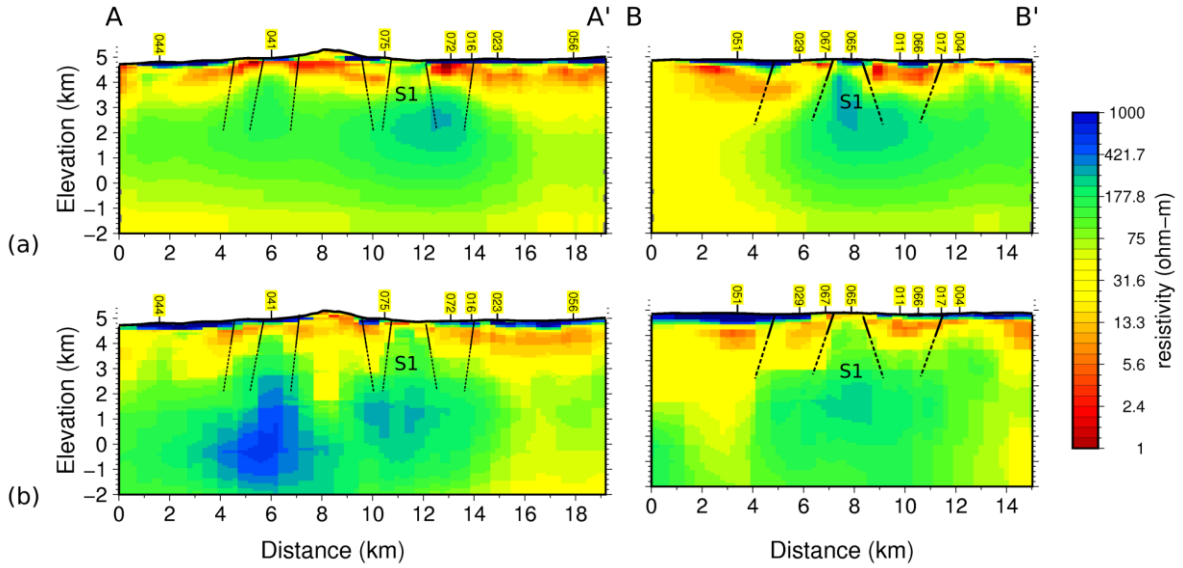

Figure 5: Vertical resistivity sections from Figure 4 extended down to -2 km asl (a) UDIP method and (b) ODIP method.

6. CONCLUSIONS

We present the results from two alternative end members 3-D inversion methods applied to a MT data from a conventional geothermal system. The first 3-D modeling of the MT data was carried out using the ModEM inversion package from Egbert and Kelbert (2012) based on an iterative nonlinear minimization approaches based on NLCG. This method, named UDIP in this study is characterised by a number of parameter much larger than the number of data. The second 3-D modeling was carried out with the Minim3D algorithm by Hautot et al. (2000,2007) based on a steepest gradient optimization method. The approach named ODIP uses a number of parameters lower than the number of data. The parameterization of the subsurface for both methods has been tested and compared. The electrical structure reveals common features found in volcanic geothermal systems. The clay cap, characterized by strong conductors was successfully recovered by both methods. The resistive structures are stronger and continuous in the models resulted from ODIP inversion, at 4,700m asl. At depth (deeper than elevation = 0 m), models generated with ODIP method present features that are absent in the models resulted from UDIP method. This happens because the second produces smoother distributions, a difficulty related to the large number of parameters. For the UDIP inversion, it is necessary to find the optimal relationship between the size of cells, number of parameters and desired misfits. A large number of cells with small dimensions produce better misfits but tends to concentrate structures at shallow regions with very high or very low resistivity values. In an attempt to fit the short and intermediate periods, it seems to penalize the longer periods, producing models with a smooth resistivity distribution at depth. The ODIP method, with much less parameters, generates blocky structures but it is able to image both shallow and deeper areas with reasonable resolution and desirable misfits. It better recovers discontinuities in the resistivity distribution, very important to identify the fault system in the area.

REFERENCES

Agencia de cooperacion international del Japon (JICA). Asistencia Especial para la implementacion del proyecto (SAPI) para el proyecto de construccion de la planta geotermica Laguna Colorada (Fase 1 de la primera etapa). *Final Report Empresa Nacional de Eletricidad* , (2015), 120p.

Avdeev, D.B. Three-dimensional electromagnetic modelling and inversion from theory to application. *Surveys in Geophysics*, **26,** (2005), 767–799.

Avdeev, D.B. and Avdeeva, A. 3d magnetotelluric inversion using a limited-memory quasi-newton optimization. *Geophysics*, **74**, (2009), F45–F57.

Bibby, H.M., Risk, G.F., Caldwell, T.G., and Heise, H. Investigations of deep resistivity structures at the wairakei geothermal field, *Geothermics*, **38,** (2009), 98 – 107. Special Issue on the Wairakei Geothermal Field, New Zealand: 50 Years Generating Electricity.

Chave, A. and Thomson, D. A bounded influence regression estimator based on the statistics of the hat matrix. *Journal of the Royal Statistical Society Series C*, **52**, (2007), 307–322.

Coppo, N., Baltassat, J.M., Girard, J.F., Wawrzyniak, P., Hautot, S., Tarits, P., Jacob, T., Martelet, G., Mathieu, F., Gadalia, A., Bouchot, V., Traineau, H. 3-D Magnetotelluric Investigations for Geothermal Exploration in Martinique (Lesser Antilles). Characteristic Deep Resistivity Structures, and Shallow Resistivity Distribution Matching Heliborne TEM Results. *Proceedings World Geothermal Congress. (*2015)

Egbert, G. and Kelbert, A. Computational recipes for electromagnetic inverse problems. *Geophysical Journal International*, **189**,(2012), 251–267.

Gao, J., Zhang, H., Zhang, S., Chen, X., Cheng, Z., Jia, X., Li, S., Fu, L., Gao, L. and Xin, H. Three-dimensional magnetotelluric imaging of the geothermal system beneath the gonghe basin, northeast tibetan plateau. *Geothermics*, **76**, (2018), 15 – 25.

Hautot, S., Tarits, P., Whaler, K.A., Le Gall, B., Tiercelin, J.J. and Le Turdu, C. Deep structure of the baringo rift basin (central kenya) from three-dimensional magnetotelluric imaging: Implications for rift evolution. *Journal of Geophysical Research*, **105**,(2000), 23493–23518.

Hautot, S., Single, R.T., Watson, J., Harrop, N., Jerram, D.A., Tarits, P., Whaler, K. and Dawes, D. 3-d magnetotelluric inversion and model validation with gravity data for the investigation of flood basalts and associated volcanic rifted margins. *Geophysical Journal International*, **170**, (2007), 1418–1430.

Hautot, S. and Tarits, P. A new coarse-to-fine 3-d magnetotelluric inversion method – application to field data for hydrocarbon exploration. **1,** (2009), 663–667.

Heise, W., Caldwell,T.G., Bibby, H.M., Bannister, S.C. Three-dimensional modelling of magnetotelluric data from the Rotokawa geothermal field, Taupo Volcanic Zone, New Zealand, *Geophysical Journal International*, **173**, (2008), 740–750.

Japan Oil, Gas and Metals National Corporation (JOGMEC). Estudio sobre Recursos Geotérmico para Suministro de Calor y Energía en la Región de Uyuni del Estado Plurinacional de Bolivia. Final *Report - Estudio de Proyectos de Infraestructura de Iniciativa Privada en Países en Desarrollo en el Año Fiscal 2010.* (2011), 384p.

Kelbert, A. Meqbel, N., Egbert, G. and Tandon, K. Modem: A modular system for inversion of electromagnetic geophysical data. *Computers & Geosciences*, **66**, (2014), 40–53.

Mackie, R.L. and Madden, T.R. Three-dimensional magnetotelluric inversion using conjugate gradients, *Geophysical Journal International*, **115**, (1993), 215–229.

Mackie, R.L., Madden. T.R. and Wannamaker, P.E. Three-dimensional magnetotelluric modeling using difference equations—theory and comparisons to integral equation solutions. *Geophysics*, **58**, (1993), 215–226.

Mackie, R.L., Smith, J,T. and Madden, T.R. Three-dimensional electromagnetic modeling using finite difference equations: The magnetotelluric example. *Radio Science*, **29,** (1994), 923–935.

Meqbel. N. The electrical conductivity structure of the Dead Sea Basin derived from 2D and 3D inversion of magnetotelluric data. *Thesys de d.sc., Freie Universit at Berlin*, Berlin, Alemanha, (2009).

Miensopust, M.P., Queralt, P., Jones, A.G. and the 3D MT modellers. Magnetotelluric 3-D inversion—a review of two successful workshops on forward and inversion code testing and comparison. *Geophysical Journal International*, **193**, (2013), 1216–1238.

Muñoz, G. , Ritter, O. and Moeck, I. A target-oriented magnetotelluric inversion approach for characterizing the low enthalpy Groß Schönebeck geothermal reservoir. *Geophysical Journal International*, **183** (2010), 1199-1215.

Muñoz, G. Exploring for geothermal resources with electromagnetic methods. *Surveys in Geophysics*, **35**, (2014), 101–122.

Newman, G.A. and Alumbaugh D.L. Three-dimensional magnetotelluric inversion using nonlinear conjugate gradients. Geophysical Journal International, **140**, (2000), 410–424.

Newman, G.A., Gasperikova, E., Hoversten, G. Wannamaker, P.E. Three-dimensional magnetotelluric characterization of the Coso geothermal field. Geothermics. **37**, (2008), 369-399.

Orris, G.J., Asher-Bolinder, S., Soria-Escalante, E., Enriquez-Romero, R. and Bailey, E.A. Laguna colorada. In U.S. Geological Survey and Servicio Geologico de Bolivia, Geology and mineral resources of the Altiplano and Cordillera Occidental, Bolivia, *Geological Survey Bulletin*, (1992), 201–202.

Di Paola, M., Luccioli, F. and G. Rico Calderon. Geothermal Feasibility Study of Laguna Colorada – Bolivia. *Technical report* **14**, 1990.

Rodi, W. and Mackie, R.L. Nonlinear conjugate gradients algorithm for 2-d magnetotelluric inversion. *Geophysics*, **66**,(2001), 174–187.

Rosenbrock, H.H. An Automatic Method for Finding the Greatest or Least Value of a Function. The Computer Journal, **3**, (1960), 175–184.

Samrock, F., Grayver, A. V., Eysteinsson, H., & Saar, M. Magnetotelluric image of transcrustal magmatic system beneath the Tulu Moye geothermal prospect in the Ethiopian Rift. *Geophysical Research Letters*, **45**, (2018), 12,847– 12,855.

SERGEOMIN. Mapa geologico de bolivia. URL http://ide.sergeomin.gob.bo/glge1msgm/, accessed in 06/05/2019.

de Silva, S.L. Altiplano-Puna volcanic complex of the central Andes. *Geology*, **17**, (1986), 1102–1106.

Siripunvaraporn, W., Egbert, G. and Lenbury, Y. Numerical accuracy of magnetotelluric modeling: A comparison of finite difference approximations. *Earth, Planets and Space*, **54,** (2002), 721–725.

Siripunvaraporn, W. Three-dimensional magnetotelluric inversion: An introductory guide for developers and users. *Surveys in Geophysics*, **33**, (2012), 5–27.

Spichak, V. and Manzella, A. Electromagnetic sounding of geothermal zones. *Journal of Applied Geophysics*, **68**, (2009), 459 – 478.

Villarroel-Camacho, D.G. Geochemical studies of geothermal fluid and evaluation of well test results from wells sm–01, sm-02 and sm–03, sol de mañana field, geothermal project, laguna colorada, bolivia. *Report Geothermal training in Iceland,* **32**, (2014), 24p.

Weaver, J.T. Mathematical Methods for Geo-electromagnetic Induction. *Applied and Engineering Mathematic Series*. Research Studies Press, Taunton, Somerset, England, 1994.